Effects of temperature- and pressure- dependent viscosity and internal heating on strongly viscous fluid like the mantle

S. A. Sayeed Motaleb[1], **Tania S. Khaleque**[1,*]

[1]Department of Applied Mathematics, University of Dhaka, Dhaka-1000, Bangladesh.

Key Points:

- Convection for high viscosity variations with low temperature cut-off viscosity.
- Relation between pressure and temperature dependent parameters in basally heated mantle.
- Comparison between convection with and without internal heating in the mantle.

Corresponding author: Tania S. Khaleque*, tania.khaleque@du.ac.bd

Abstract

A mathematical model is considered for Rayleigh-Bénard convection of mantle whose viscosity depends strongly both on temperature and pressure defined in an Arrhenius form. The model is solved numerically for extremely large viscosity variations across a unit aspect ratio cell, and steady solutions are obtained. To improve the efficiency of numerical computation, a modified viscosity law with a low temperature cut-off is used. The aim is to investigate the convection pattern with internal heating at a very high viscosity variation in the presence of high Rayleigh number. The study also investigates the relation between temperature-dependent parameter and pressure dependent parameter. The numerical simulation is done using the finite element method based PDE solver and the results are presented through figures, tables and graphs.

Plain Language Summary

Convection is a process where the heat is transferring from one place to another caused by the movement of the fluid particles. The inner infrastructure of the Earth can be divided into Center, Core, Mantle and Crust. The surface of the Earth is the part of crust and the molten materials that lies beneath the crust is known as Mantle which is about 84% of the Earth's total volume. Mantle Convection can be defined as the process where hot materials sink and cool materials rise up, this loop process is responsible for plate tectonic movement, volcanic eruptions, earthquakes, etc. The mantle is powered by the core but also there is some rocks in the mantle which are capable of providing the heat necessary to occur the convection. That's why we are interested about the internal heating in the mantle. Also, as we go deeper not only temperature but also pressure dependence parameter becomes significant and so we want to study these dependence on viscosity and understand how it affects the mantle convection.

1 INTRODUCTION

Mantle convection in the Earth and other planets is a complex mechanism. It sets the pace for the evolution of the Earth as a whole. It is the primary mechanism for the transport of heat from the Earth's deep interior to its surface and the fundamental cause of plate tectonics, formation and drift of continents, volcanism, earthquakes, and mountain building Schubert et al. (2001). There are two possible heat sources to drive this convection: the primary sources of thermal energy for mantle convection are internal heating due to the

decay of the radioactive isotopes of uranium, thorium, and potassium, the long-term secular cooling of the Earth, and heat from the core Schubert et al. (2001). Mantle convection is also very much influenced by its enormous viscosity. The effective viscosity of the mantle is a strong function of temperature, pressure, and stress. The temperature and stress dependences are well documented experimentally. The first attempt to model mantle convection was made by D. Turcotte and Oxburgh (1967). They performed a boundary-layer analysis of two-dimensional steady state convection of a constant viscosity fluid at high Rayleigh number. Later Roberts (1977), Olson and Corcos (1980), Jimenez and Zufiria (1987) presented improved boundary layer analyses for mantle convection. The temperature-dependent case was studied numerically by Christensen (1984), Christensen (1984b), Moresi and Solomatov (1995), Solomatov and Moresi (1997), Kameyama and Ogawa (2000). The influence of temperature and depth-dependent viscosity on convection has been explored in two-dimensional numerical experiments by Houston and De Bremaecker (1975), Christensen (1984b), Fleitout and Yuen (1984), Doin et al. (1997), Dumoulin et al. (1999), Stemmer et al. (2006), Khaleque et al. (2015). The work involving 'internal heating' is investigated by Bercovici et al. (1989), Ito and Katsura (1989), Leitch et al. (1991), Davies and Richards (1992), Bercovici et al. (2000), D. L. Turcotte and Schubert (2002), Van Heck and Tackley (2011), Stein et al. (2013), Limare et al. (2015), King (2015), Korenaga (2017).

In this paper, we present numerical results of Rayleigh-Bénard convection influenced by variable viscosity (Khaleque et al., 2015) which depends strongly on both temperature and pressure with the presence of internal heating. This type of Arrhenius law with an imposed cut off viscosity was applied by Huang et al. (2003), Huang and Zhong (2005) and King (2009) but none of them was applied to a temperature and pressure dependent viscosity. Khaleque et al. (2015) applied this cut-off viscosity function to a temperature and pressure dependent viscosity and emphasises that this trick enables numerical simulation of the extreme viscosity variations without compromising anything. In Sec. 2, we introduce and nondimensionalize the governing equations and boundary conditions. We validate our method through comparison with benchmark values and then present our numerical results with internal heating in Sec. 4 by graphs and tables. A discussion on the relationship between temperature and pressure dependent parameters is also presented here. A comparison is shown between 'with' and 'without' internal heating which follows in Sec. 5 and finally, we draw our conclusions in Sec. 6.

2 GOVERNING EQUATIONS

2.1 Model equations and boundary conditions

We consider classical Rayleigh-Bénard convection in a two-dimensional square cell with a fixed temperature difference ΔT between the horizontal boundaries. This convective cell is assumed to be a part of a periodic structure in an infinite horizontal layer. We adopt Cartesian coordinates (x, z) with the x-axis horizontal and the z-axis pointing vertically upwards. The governing equations which describe the motion are (is treated as a *Boussinesq fluid*),

$$\begin{aligned} \rho\nabla\cdot(\boldsymbol{u}) &= 0, \\ \rho\left[\frac{\partial \boldsymbol{u}}{\partial t} + (\boldsymbol{u}.\nabla)\boldsymbol{u}\right] &= -\nabla p + \nabla\cdot\boldsymbol{\tau} - \rho g\hat{\boldsymbol{k}}, \\ \boldsymbol{\tau} = \eta[\nabla\boldsymbol{u} + (\nabla\boldsymbol{u})^T], \quad \boldsymbol{\tau}^2 &= \tau_1^2 + \tau_3^2, \\ \rho &= \rho_0[1-\alpha(T-T_b)], \\ \rho C_p\left[\frac{\partial T}{\partial t} + \boldsymbol{u}.\nabla T\right] &= \kappa\nabla^2 T + \frac{\tau^2}{2\eta} + \rho Q, \end{aligned} \tag{2.1}$$

where, $\boldsymbol{u} = (u, 0, w)$ is the fluid velocity, t is time, p is the pressure, ρ is the density, $\boldsymbol{\tau}$ is the deviatoric stress tensor, τ_1 and τ_3 are longitudinal and shear components of the deviatoric stress respectively, T is the absolute temperature, and η is the viscosity. The parameters in the equations are the constant gravitational acceleration acting downward g, specific heat at constant pressure C_p, thermal conductivity κ, (radiogenic) internal heating Q, thermal expansion coefficient α, reference density ρ_0, basal temperature T_b. In general, η is a function of temperature, pressure and stress which is written as,

$$\eta = \frac{1}{2A(\tau_1^2+\tau_3^2)^{(n-1)/2}} exp\left(\frac{E+pV}{RT}\right), \tag{2.2}$$

where A is the rate factor, n is the flow index, E is the activation energy, V is the activation volume, and R is the universal gas constant. This form of viscosity function is known as Arrhenius form of viscosity.

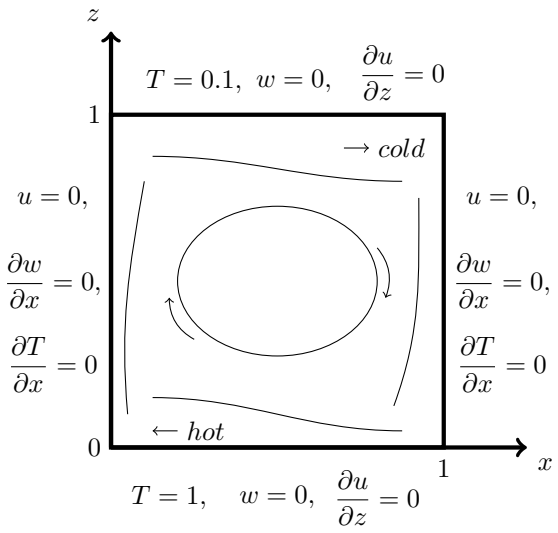

Figure 1: Schematic diagram of a basally heated non-dimensional unit aspect-ratio cell in mantle.

We will consider only two-dimensional motion in the (x, z) plane. We impose the free-slip boundary conditions on all boundaries and thermal insulation on the vertical sides. The top and bottom are maintained at specified temperatures T_s and T_b respectively, so the boundary conditions are,

$$\begin{aligned} w &= 0, \quad \frac{\partial u}{\partial z} = 0, \quad T = T_b \quad on \quad z = 0, \\ w &= 0, \quad \frac{\partial u}{\partial z} = 0, \quad T = T_s \quad on \quad z = d, \\ u &= 0, \quad \frac{\partial u}{\partial z} = 0, \quad T_x = 0 \quad on \quad x = 0, d. \end{aligned} \tag{2.3}$$

where d is the depth. In addition, we consider only Newtonian rheology, and therefore set $n = 1$ in (2.2).

2.2 Non-dimensionalisation

Following Fowler (2011), Jarvis and Peltier (1982), we non-dimensionalize as follows:

$$\begin{gathered} (x, z) = d(x^*, z^*), \quad T = \Delta T T^* + T_s, \quad \boldsymbol{u} = \frac{\kappa_0}{d}\boldsymbol{u}^*, \quad t = \frac{d^2}{\kappa_0}t^* \\ \eta = \frac{e^{(1+\mu)/\epsilon}}{2A}\eta^*, \quad \rho = \rho_0\rho^*, \quad \tau = \frac{\eta_0\kappa_0}{d^2}\tau^*, \quad p = \rho g d(1 - z^*) + \frac{\eta_0\kappa_0}{d^2}p^* \end{gathered} \tag{2.4}$$

Substituting these variables in equations (2.1),(2.2), we obtain the following dimensionless equations by dropping the asterisks:

$$\begin{aligned} \frac{\partial u}{\partial x} + \frac{\partial w}{\partial z} &= 0, \\ \frac{1}{Pr}\rho\left[\frac{\partial \boldsymbol{u}}{\partial t} + (\boldsymbol{u}.\nabla)\boldsymbol{u}\right] &= -\nabla p + \nabla\cdot\boldsymbol{\tau} - Ra(1-T)\hat{\boldsymbol{k}}, \\ \frac{\partial T}{\partial t} + \boldsymbol{u}.\nabla T &= \nabla^2 T + \frac{D}{Ra}\frac{\tau^2}{2\eta} + H, \end{aligned} \tag{2.5}$$

where, $\boldsymbol{\tau} = \eta[\nabla\boldsymbol{u} + (\nabla\boldsymbol{u})^T] = \eta\nabla\boldsymbol{u}$. While the dimensionless version of constitutive η relation with $n = 1$ leads to,

$$\eta = exp\left[\frac{1 - T + \mu(1 - z - T) + \bar{B}p/Ra}{\epsilon T}\right], \tag{2.6}$$

where the dimensionless parameters are,

Dimensionless surface tempearture,	$\theta_0 = \frac{T_s}{T_b}$,	Prandtl number,	$Pr = \frac{\eta_0}{\rho_0\kappa_0}$,
Dissipation number,	$D = \frac{\alpha g d}{C_p}$,	Viscous pressure number,	$\mu = \frac{\rho_0 g d v}{E}$,
Internal heating number,	$H = \frac{\rho_0 Q d^2}{\kappa_0 T_b}$,	Viscous temperature number,	$\epsilon = \frac{RT_b}{E}$,
Rayleigh number,	$Ra = \frac{\rho_0\alpha g\Delta T d^3}{\eta_0\kappa_0}$,	Boussinesq number,	$\bar{B} = \alpha T_b$.

Using the typical parameter values for the mantle as shown in Table 1, we find that $Pr \approx 10^{23}$ and $D \approx 0.6$. Thus, Pr can be taken as infinite and for $Ra \gg 1$, D/Ra can be neglected. $\bar{B}/Ra$ can easily be ignored in the viscosity relation. However, we are going to use a low-temperature cut-off viscosity function (Khaleque et al., 2015) defined as follows,

$$\eta = \begin{cases} exp[M/\epsilon] & , M \le \epsilon\ log10^6 \\ 10^6 & , \text{otherwise}, \end{cases} \tag{2.7}$$

where,

$$M = \frac{(1+\mu)(1-T) - \mu z}{T}. \tag{2.8}$$

Here, ϵ is the viscous temperature number and μ is the viscous pressure number. The heating parameter H depends on the assumed distribution of radioactive elements in the mantle. If we take thermal conductivity to be constant ($\kappa = 1$), then we obtain the dimensionless Boussinesq equations of convection,

$$\begin{aligned} \nabla\cdot\boldsymbol{u} &= 0, \\ \nabla p &= \nabla\cdot(\eta\nabla\boldsymbol{u}) - Ra(1-T)\hat{\boldsymbol{k}}, \\ \frac{\partial T}{\partial t} + \boldsymbol{u}.\nabla T &= \nabla^2 T + H, \end{aligned} \tag{2.9}$$

The associated free-slip dimensionless boundary conditions are,

$$\begin{aligned} w = 0, \quad \frac{\partial u}{\partial z} = 0, \quad T = 1 \quad on \quad z = \quad 0, \\ w = 0, \quad \frac{\partial u}{\partial z} = 0, \quad T = \frac{T_s}{T_b} = \theta_0 \quad on \quad z = \quad 1, \\ u = 0, \quad \frac{\partial w}{\partial x} = 0, \quad T_x = 0 \quad on \quad x = \quad 0, 1. \end{aligned} \tag{2.10}$$

Our complete dimensionless model consists of governing equations (2.9), constitutive relation (2.7),(2.8) and boundary conditions (2.10).

2.3 Viscosity contrast, Nusselt number and Root means square (RMS) velocity

We define three useful diagnostic quantities which will be used to characterise the numerical results found. First, we define the viscosity contrast $\Delta\eta$ to be the ratio between the surface and basal values (bottom layer values) of the viscosity, that is,

$$\Delta\eta = exp\left(\frac{1 - \theta_0 - \mu\theta_0}{\epsilon\theta_0}\right). \tag{2.11}$$

Second, the Nusselt number Nu is the ratio of the average surface heat flow from the convective solution to the heat flow due to conduction and is calculated in the present case of a square cell by the dimensionless relation

$$Nu = -\frac{1}{a(1-\theta_0)} \int_0^a \frac{\partial T}{\partial z}(x, 1)\, dx. \tag{2.12}$$

Finally, the vigour of the circulating flow is characterised by the non-dimensional RMS velocity, defined by

$$V_{rms} = \left[\int_0^1 \int_0^a (u^2 + w^2)\, dx\, dz\right]^{1/2}. \tag{2.13}$$

In our case, $a = 1$ and $\theta_0 = 0.1$.

Table 1: Typical parameter values for numerical models of mantle convection.

Parameter	Symbol	Value
Mantle Depth	d	3×10^6 m
Thermal expansion coefficient	α	2×10^{-5} K^{-1}
Reference density	ρ_o	4×10^3 kgm^{-3}
Gravitational acceleration	g	10 ms^{-2}
Temperature at the base of the lithosphere	T_s	300 K
Temperature at the core-mantle boundary	T_b	3000 K
Temperature difference	ΔT	2700 K
Thermal conductivity	κ_o	4 W m^{-1}K^{-1}
Specific heat at constant pressure	C_p	10^3 J Kg^{-1} K $^{-1}$
Thermal diffusivity coefficient	$\kappa_o = \frac{\kappa_o}{\rho_o C_p}$	1×10^{-6} m^{2}s^{-1}
Dynamic viscosity	η_0	10^{21} Pa s
Rayleigh number	Ra	$10^4 - 10^7$
Activation energy	E	$300 - 525$ kJmol^{-1}
Activation volume	V	6×10^{-6} m^{3}mol^{-1}
Universal gas constant	R	8.31 Jmol^{-1}K^{-1}
Viscous rate constant	A	10^5 MPa^{-1}s^{-1}
Viscous temperature number	ϵ	$0.042 - 0.083$
Viscous pressure number	μ	$1.2 - 2.4$
Boussinesq number	$\bar{B}$	0.06
Dimensionless surface temperature	θ_0	0.1

3 METHODOLOGY

3.0.1 Comparison with Benchmark values

To validate our model, we first solve the model in a unit aspect ratio cell ($a = 1$) setting $\eta = 1$, $H = 0$ and $\theta_0 = 0$. i.e. we consider constant viscosity. We use a finite element method based PDE solver *'COMSOL Multiphysics'* to solve numerically the dimensionless governing equations (2.9)-(2.10). To build our model the physics of creeping fluid flow, heat transfer in fluids and Poisson's equation are coupled. We choose the appropriate free triangular meshing with some refinement near the boundaries. As for the basis functions

or shape functions, we select Lagrangian P2-P1 elements for creeping flow which means the shape functions for the velocity field and pressure are Lagrangian quadratic polynomials and Lagrangian linear polynomials, respectively. Similarly, Lagrangian quadratic elements for both temperature in the heat equation and the streamfunction in Poisson's equation are chosen. Our specific discretization finally produces 150,267 degrees of freedom (N_{dof}). We have compared the values of Nusselt number, Nu and root mean square velocity, V_{rms} with the benchmark values from Blankenbach et al. (1989) and Koglin Jr et al. (2005) for mantle convection with constant viscosity. Their values were computed for Ra up to 10^6 and 10^7 respectively. The comparison is shown in Table 2, where we can observe that the agreement is within a very good range.

Table 2: Comparison of Nusselt number, Nu and RMS velocity, V_{rms} for constant viscosity with benchmark values from (Blankenbach et al., 1989)[a] and (Koglin Jr et al., 2005)[b]

Ra	Nu			V_{rms}		
	Benchmark	This work	Error(%)	Benchmark	This work	Error(%)
10^4	4.884409[a]	4.88441	0.00002	42.864947[a]	42.86497	0.00005
10^5	10.534095[a]	10.53409	0.00005	193.21454[a]	193.21548	0.00047
10^6	21.972465[a]	21.97245	0.00007	833.98977[a]	834.00658	0.00202
10^7	45.62[b]	45.63173	0.03	....	3634.04868	....

4 Numerical Simulation of Mantle Convection with Internal Heating

4.1 Simulation Results and Discussion

We solve the system of dimensionless equations (2.9) with the boundary conditions (2.10) by setting $H = 0.0, 2.0, 3.0, 5.0, 6.0$, along with the cut-off viscosity function defined as in equations (2.7) and (2.8), so that the viscosity depends strongly both on temperature and pressure.

Table 3: Comparison of Nusselt number, Nu and RMS velocity, V_{rms} with values from (Khaleque et al., 2015), using cutoff viscosity function at Ra= 10^7 and $\theta_0 = 0.1$, $H = 0.0$.

$\Delta\eta$	μ	ϵ	Nu		V_{rms}	
			This work	Khaleque *et al.*	This work	Khaleque *et al.*
10^{10}	0.5	0.369	8.0632	8.04491	1000.2615	999.9255
	1.0	0.3474	9.3392	9.31593	1189.7667	1186.3094
10^{15}	0.5	0.246	6.9647	6.95366	893.4528	892.7446
	1.0	0.2316	8.1909	8.17339	957.8617	956.18565
10^{20}	0.5	0.1846	6.2722	6.25907	806.0677	804.45323
	1.0	0.1737	6.8964	6.89670	610.1082	614.08143
10^{25}	0.5	0.1477	5.7638	5.75448	721.55095	720.1903
	1.0	0.139	5.4793	5.49674	315.2551	317.69797
10^{30}	0.5	0.123	5.3457	5.3509	634.03108	634.18688
	1.0	0.1158	4.8863	4.9234	278.0535	273.45468

We compare our results with (Khaleque et al., 2015) for $H = 0.0$ and found a good agreement with them, which is presented in Table 3. The simulation results are presented by temperature distributions and stream function contours mainly. At first we present the temperature distributions. At each plot of the temperature profile, the blue region corresponds to the cooler temperature whereas the red region corresponds to the high temperature. The cold upper thermal boundary layer represents the stagnant lid. Since, the fluid has a viscosity which depends strongly on temperature and pressure it is no longer possible for the

bulk flow to be both isothermal and isoviscous. From Figure 2, when $\mu = 0.5$, we observe that as ϵ decreases (i.e, viscosity contrast $\Delta\eta$ increases) the thickness of the lid increases.

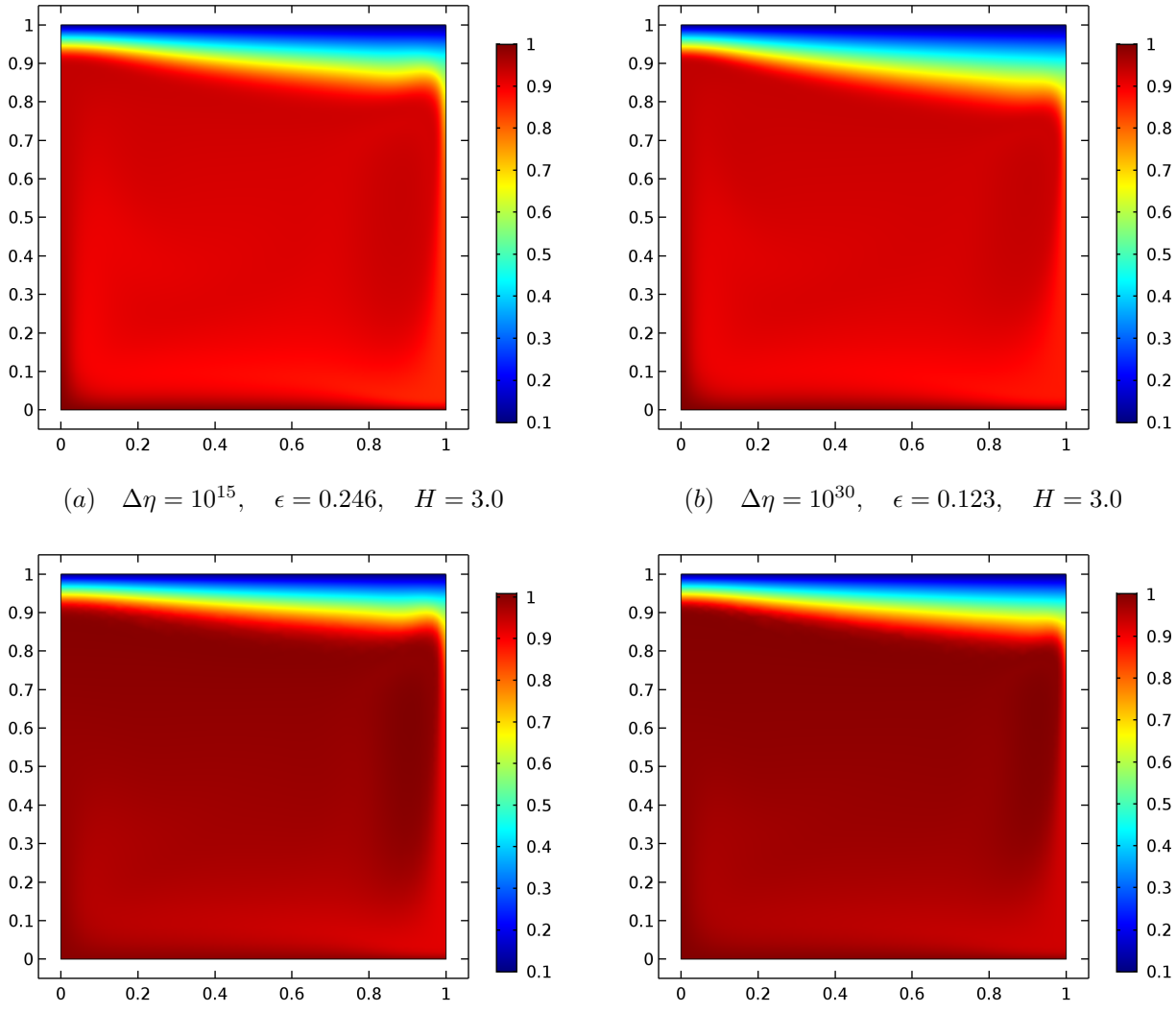

(a) $\Delta\eta = 10^{15}$, $\epsilon = 0.246$, $H = 3.0$

(b) $\Delta\eta = 10^{30}$, $\epsilon = 0.123$, $H = 3.0$

(c) $\Delta\eta = 10^{15}$, $\epsilon = 0.246$, $H = 6.0$

(d) $\Delta\eta = 10^{30}$, $\epsilon = 0.123$, $H = 6.0$

Figure 2: Thermal distributions of a temperature and pressure dependent viscosity convection at different viscosity contrast, where $\mu = 0.5$ and $H = 3.0, 6.0$, with $\theta_0 = 0.1$ and $Ra = 10^7$.

At the lower mantle near the core mantle boundary, the temperature is higher as expected and this temperature is also increasing as the viscosity contrast gets larger. The temperature associated with the lower mantle and near the core mantle boundary at $H = 6.0$ is greater than the temperature associated with the core, the lower mantle and near the core mantle boundary at $H = 3.0$.

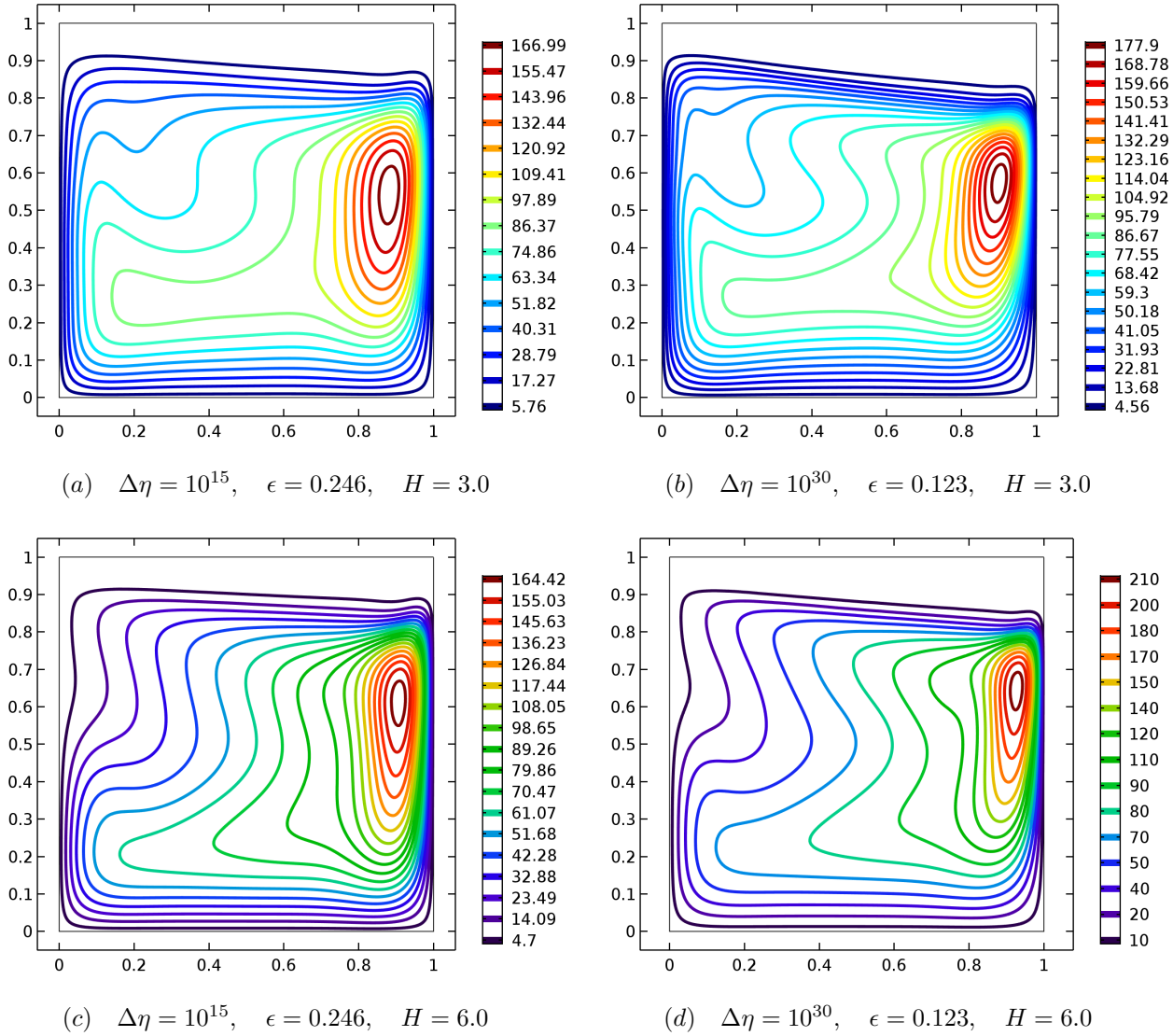

(a) $\Delta\eta = 10^{15}$, $\epsilon = 0.246$, $H = 3.0$

(b) $\Delta\eta = 10^{30}$, $\epsilon = 0.123$, $H = 3.0$

(c) $\Delta\eta = 10^{15}$, $\epsilon = 0.246$, $H = 6.0$

(d) $\Delta\eta = 10^{30}$, $\epsilon = 0.123$, $H = 6.0$

Figure 3: Stream function contours of a temperature and pressure dependent viscosity convection at different viscosity contrast, where $\mu = 0.5$ and $H = 3.0, 6.0$, with $\theta_0 = 0.1$ and $Ra = 10^7$.

When $\mu = 1.0$, we observe the appearance of quite a different flow structure in Figure 4. The interior temperature is significantly lower than the case with $\mu = 0.5$. That means strong pressure dependence in the viscosity function reduce the internal temperature.

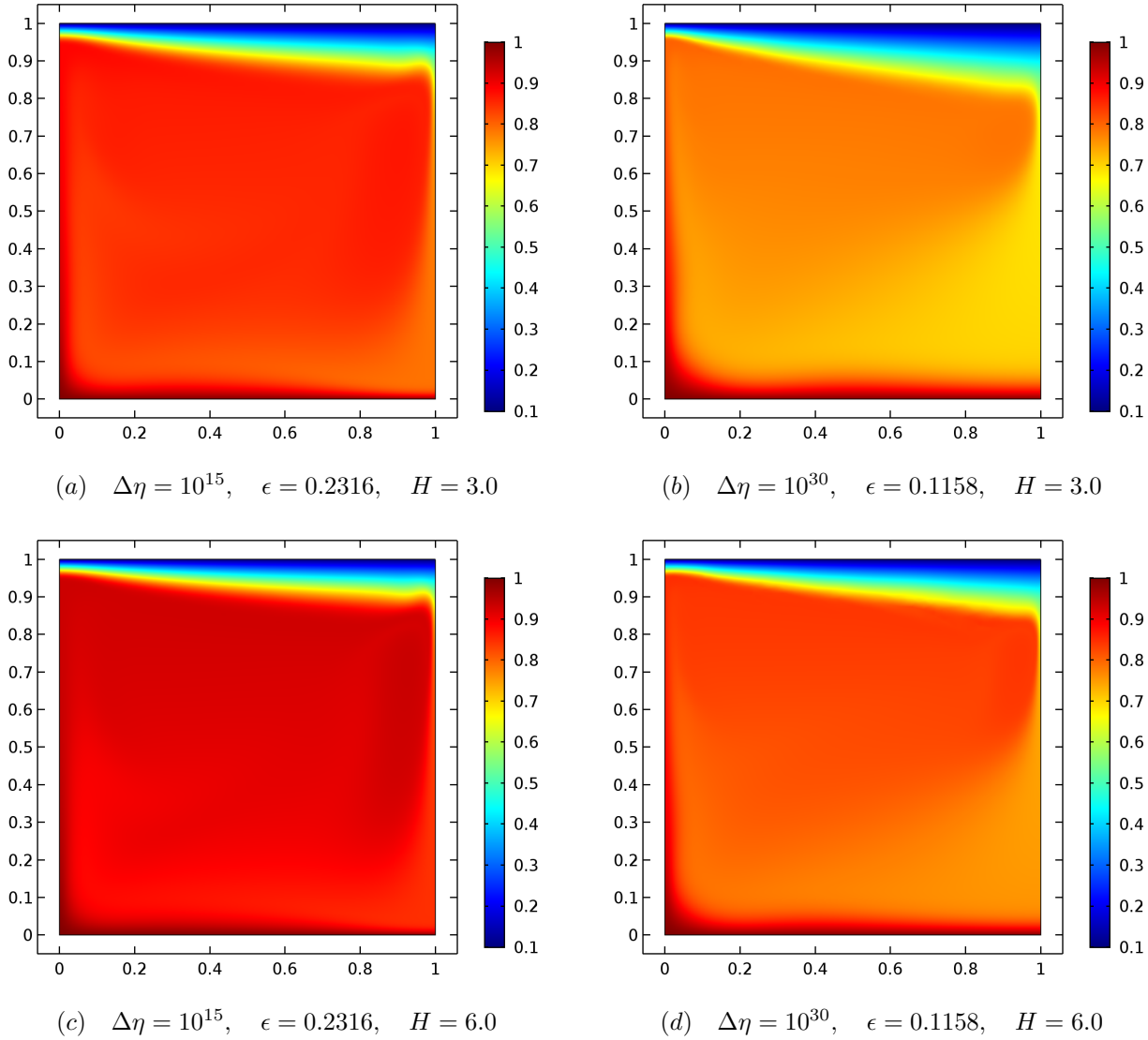

(a) $\Delta\eta = 10^{15}, \quad \epsilon = 0.2316, \quad H = 3.0$

(b) $\Delta\eta = 10^{30}, \quad \epsilon = 0.1158, \quad H = 3.0$

(c) $\Delta\eta = 10^{15}, \quad \epsilon = 0.2316, \quad H = 6.0$

(d) $\Delta\eta = 10^{30}, \quad \epsilon = 0.1158, \quad H = 6.0$

Figure 4: Thermal distributions of a temperature and pressure dependent viscosity convection at different viscosity contrast, where $\mu = 1.0$ and $H = 3.0, 6.0$, with $\theta_0 = 0.1$ and $Ra = 10^7$.

The corresponding streamlines are also presented in Figure 3 and Figure 5. In each case of the streamfunction contours, the absence of streamlines at the top indicates the presence of a stagnant lid, but the overall convection pattern changes markedly as viscosity gets larger and also as the internal heating is increasing.

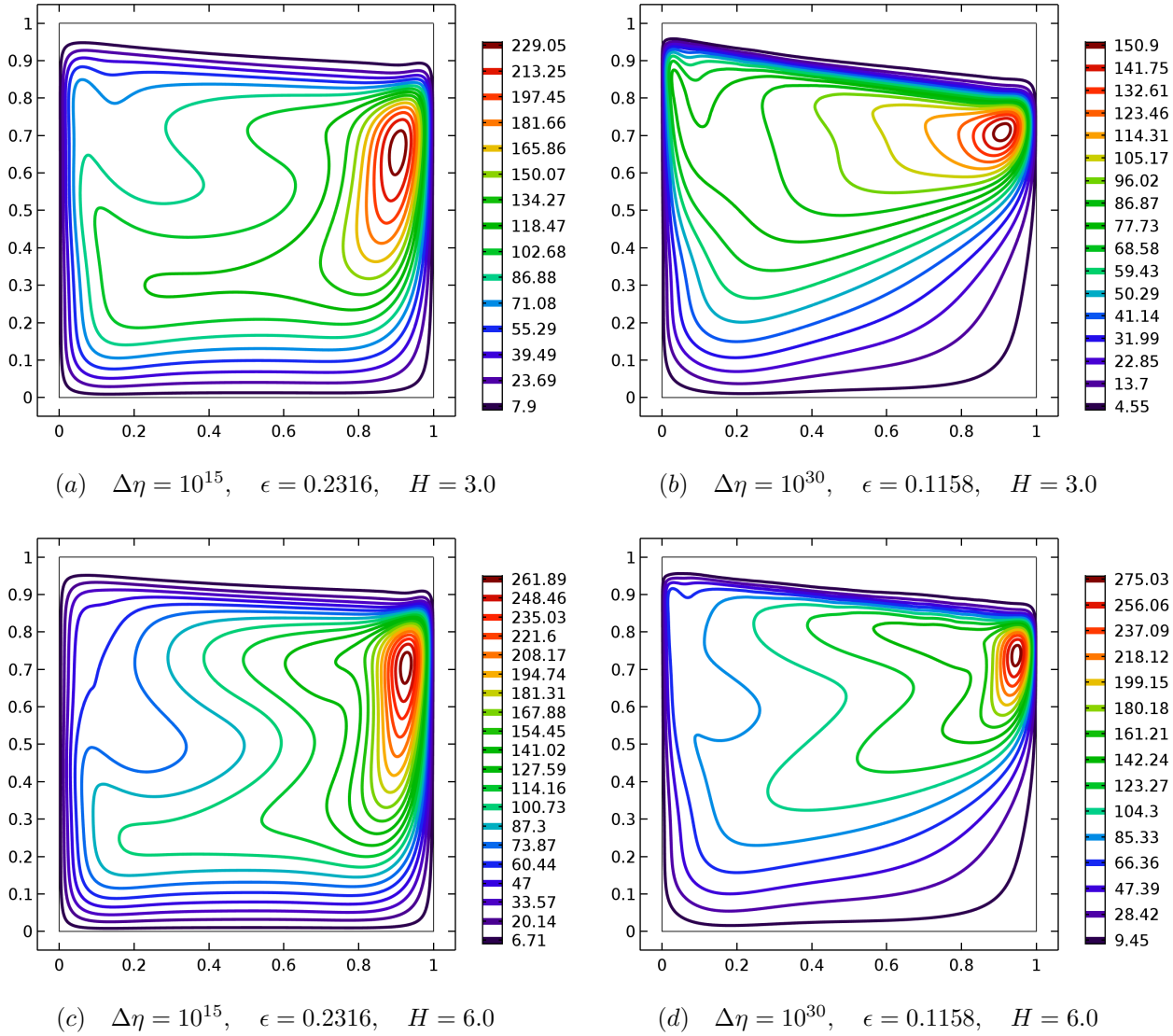

(a) $\Delta\eta = 10^{15}$, $\epsilon = 0.2316$, $H = 3.0$

(b) $\Delta\eta = 10^{30}$, $\epsilon = 0.1158$, $H = 3.0$

(c) $\Delta\eta = 10^{15}$, $\epsilon = 0.2316$, $H = 6.0$

(d) $\Delta\eta = 10^{30}$, $\epsilon = 0.1158$, $H = 6.0$

Figure 5: Stream function contours of a temperature and pressure dependent viscosity convection at different viscosity contrast, where $\mu = 1.0$ and $H = 3.0, 6.0$, with $\theta_0 = 0.1$ and $Ra = 10^7$.

Next, we plot the temperature profiles at the mid-cell (i.e. $x = 0.5$) for different viscosity contrasts. In Figures 6(a,b), we show how temperature changes with depth. The Figure 6(a) shows that the temperature changes mainly in the upper part of the mantle. In the middle the temperature is almost constant for $H = 6.0$ approximately. In Figure 6(b), we plot mid-cell temperature profiles for $\mu = 1$ presented with internal heating. We see that when $\mu = 1$, the interior temperature is no longer constant. The temperature is significantly

lower than with $\mu = 0.5$. It is also clear that that the mid-cell temperature decreases in the interior as the viscosity contrast gets larger.

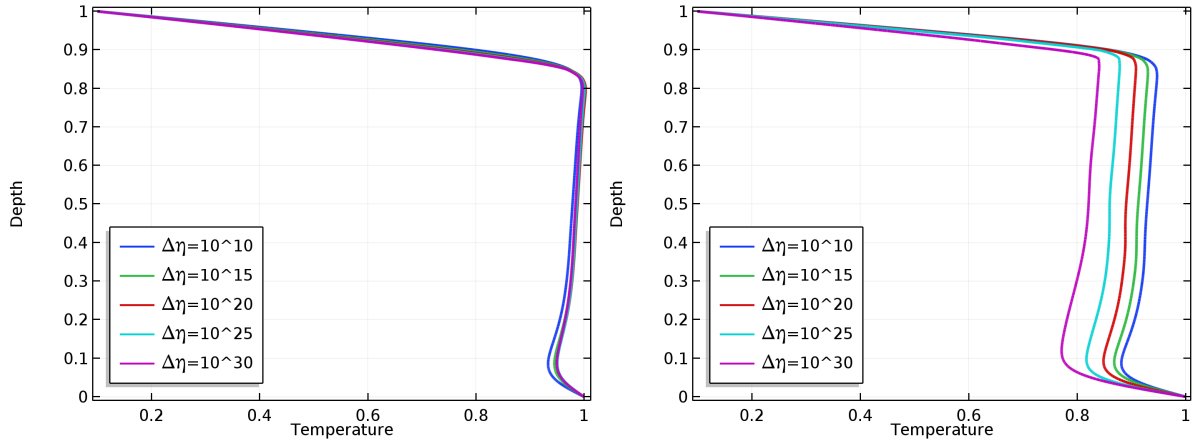

(a) $\mu = 0.5, \quad \epsilon = .123, \quad H = 6.0$ (b) $\mu = 1.0, \quad \epsilon = .1158, \quad H = 6.0$

Figure 6: Temperature profiles of mid-cell at different viscosity contrasts due to varying ϵ for convection with temperature and pressure-dependent viscosity with internal heating at $\theta_0 = 0.1$ and $Ra = 10^7$.

In Tables 4, we present the values of the Nusselt number, Nu and the root mean square velocity, V_{rms} with the variation of internal heating parameter at two pressure dependent parameter values, $\mu = 0.5, 1.0$. At a fixed pressure dependence parameter μ, we are interested to see how Nusselt number, Nu and root mean square velocity, V_{rms} change with decrease of temperature dependent parameter, ϵ and with the increase of internal heating. We keep the pressure dependence parameter μ fixed and the temperature dependence parameter ϵ is decreased and as a result variation of viscosity across the layer is increased. We observe form Tables 4 that, as the viscosity contrast increases the values of Nu decreases. When $\mu = 0.5$, Nu decreases as viscosity variation gets larger however when $\mu = 1.0$ with $H = 5.0, 6.0$, Nu shows an irregular pattern of decreasing. However root mean square velocity shows a different situation, it seems they are decreasing at first sight however the RMS velocity is increasing as $\Delta\eta$ increases at $\mu = 0.5$.

Table 4: Values of Nusselt number, Nu and RMS velocity, V_{rms} using cutoff viscosity function with internal heating at Ra= 10^7 and $\theta_0 = 0.1$.

$\Delta\eta$	μ	ϵ	$H = 3.0$		$H = 5.0$		$H = 6.0$	
			Nu	V_{rms}	Nu	V_{rms}	Nu	V_{rms}
10^5	0.5	0.7383	9.7032	606.3496	9.9802	543.7896	10.1055	518.2479
	1.0	0.695	10.5357	694.0388	11.0337	647.4956	11.1469	626.2557
10^{10}	0.5	0.369	8.0192	551.4930	8.4323	513.1509	8.8891	506.0699
	1.0	0.3474	9.5584	721.2400	10.3346	726.7835	10.6781	731.2395
10^{15}	0.5	0.246	7.3182	538.0019	7.9273	527.7812	8.4293	530.9498
	1.0	0.2316	9.3135	769.4341	10.3797	846.3291	10.8844	883.2726
10^{20}	0.5	0.1846	6.9399	539.9098	7.6989	559.0451	8.2252	573.5983
	1.0	0.1737	9.0747	790.1099	10.4245	962.5116	11.0230	1041.4943
10^{25}	0.5	0.1477	6.7237	549.5528	7.6053	600.4647	8.1282	630.4403
	1.0	0.139	8.4535	711.6921	10.0820	993.7598	10.6301	1106.7552
10^{30}	0.5	0.123	6.5912	562.3468	7.5402	648.8595	8.0349	691.7370
	1.0	0.1158	7.3769	540.4424	8.9379	804.4197	9.4438	917.9902

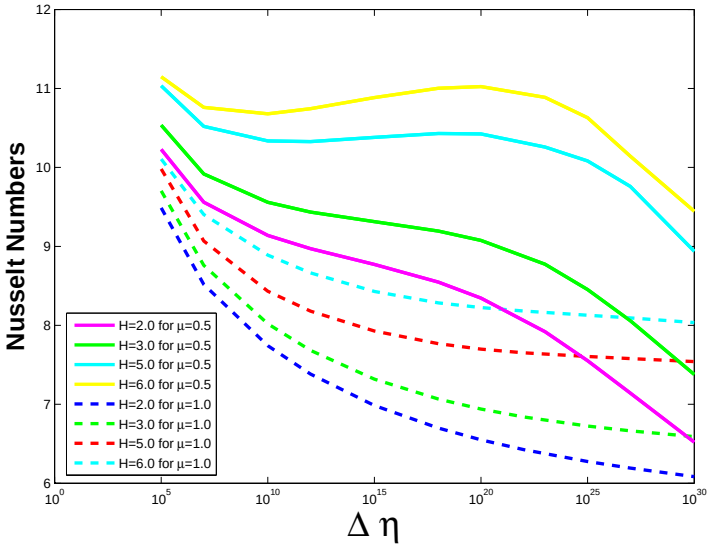

Figure 7: Variation of Nusselt number Nu with viscosity contrast $\Delta\eta$ in a unit aspect-ratio cell for $\mu = 0.5$(dashed line) and $\mu = 1.0$ with $\theta_0 = 0.1$ and $Ra = 10^7$.

In Figure 7, we plot the variation of the Nusselt number Nu versus viscosity contrast $\Delta\eta$ for $H = 2.0, 3.0, 5.0, 6.0$. From 7, we observe that as the viscosity contrast increases the values of the Nu decrease and show a smoothly decreasing pattern for $\mu = 0.5$, however, when viscosity is strongly dependent on pressure, i.e. when $\mu = 1.0$, Nu shows an irregular decreasing pattern. We also observe from Figure 7, that when the values of H is increasing, the values of the Nu is also increasing, it means the convection becomes more dominant for higher values of internal heating.

4.2 Variation of pressure dependence parameter μ

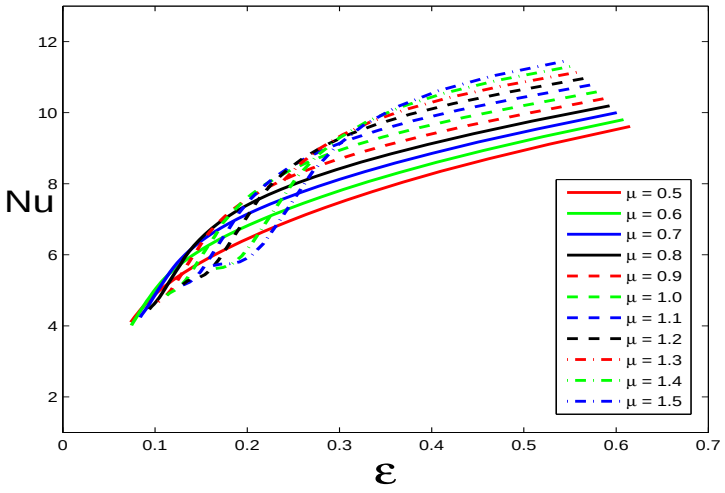

Figure 8: Variation of Nusselt number Nu with temperature parameter ϵ at different pressure sensitivity μ values in a square cell with $T_0 = 0.1$ and $Ra = 10^7$.

With this new form of viscosity function, we are able to run simulations for a larger range of μ values. In Figure 8, the Nusselt number Nu is plotted against ϵ for various μ values. For a fixed value of μ, Nu decreases as ϵ decreases. This is expected as decrease of ϵ corresponds to increase of viscosity contrast across the mantle. It should be noted that for the same viscosity contrast where $\Delta\eta < 10^9$ or $\epsilon > 0.35$, Nu gets large with the increase of μ. However, the qualitative behaviour of the curves exhibits a significant change with the increase of μ. To get a better understanding, we also plotted Nu versus $\Delta\eta$ for various values of μ in Figure 9. When μ is around $0.5 \sim 0.6$, the value of Nu decreases steadily with

the increase of viscosity variation. However, as μ increases, there comes a point where the curve changes its behaviour quite abruptly, i.e. Nu undergoes a rapid decrease and becomes a decreasing function of μ for very small values of ϵ (or for large viscosity contrasts $\Delta\eta$). Also for bigger values of μ, this point of sudden change comes at larger values of ϵ, i.e. at smaller viscosity variations. From Figure 9, we observe that the highest values of Nu at a certain viscosity contrast creates a type of envelope. Similarly, we also observe that the lowest values of Nu when strong pressure dependence is present, creates a log-linear relation with $\Delta\eta$. The line can be best approximated by

$$Nu = 7 - 0.07\log(\Delta\eta), \tag{4.1}$$

which is shown in Figure 9.

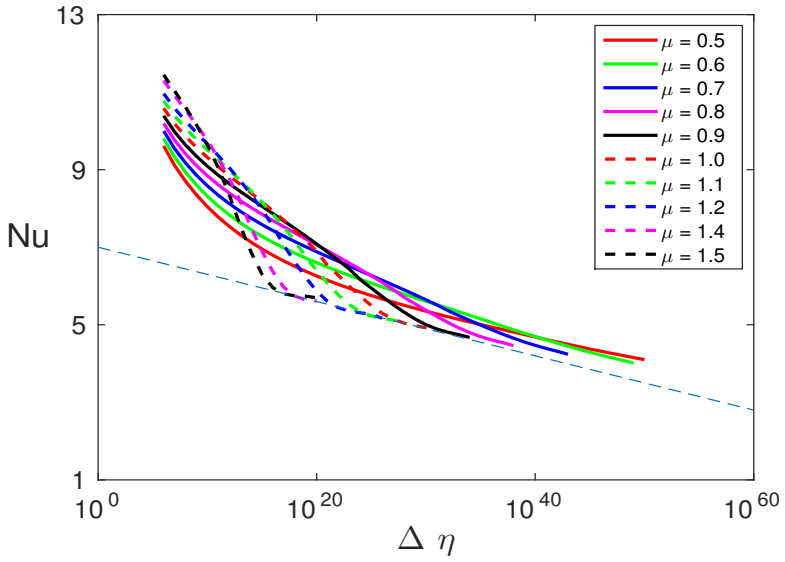

Figure 9: Variation of Nusselt number Nu with viscosity contrast $\Delta\eta$ at different pressure sensitivity μ values in a square cell with $T_0 = 0.1$ and $Ra = 10^7$. The dashed line is the envelope approximation given by (4.1).

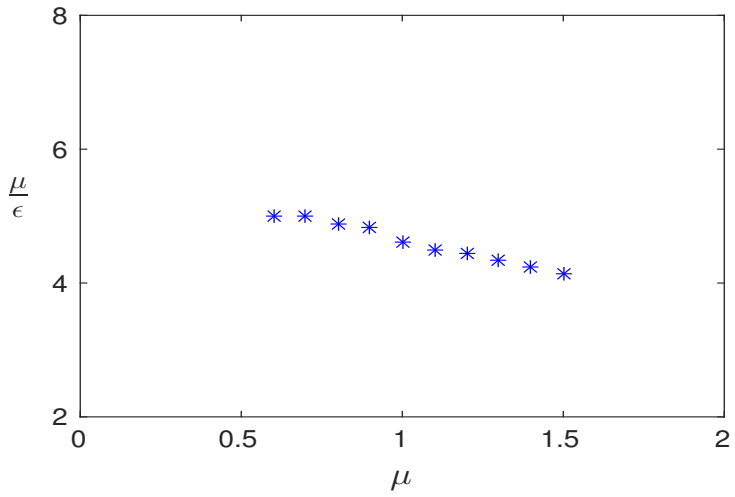

Figure 10: Variation of the ratio μ/ϵ with μ. The values of ϵ are chosen from Figure 8 where the Nusselt number Nu starts to decrease rapidly.

In Figure 10, we have plotted the values of μ/ϵ versus μ, where the values of ϵ for each μ are chosen from Figure 8 at which the value of Nu starts to decrease rapidly. The graph is consistent with the idea that the transition in behaviour is associated with going from $\mu = O(1)$ to $\mu = O(\epsilon)$ or vice-versa. The variation of Nu with ϵ and μ is quite extra-ordinary in qualitative manner. No such pattern can be seen when internal heating is considered. It is difficult to explain the exact reason behind this behaviour. However, to make a comment on it, we have presented some results of thermal distributions and logarithmic viscosity distributions at viscosity contrasts of 10^{10}, 10^{16} and 10^{20} for a fixed value of $\mu = 1.5$ in Figure 11. We observe that at $\Delta\eta = 10^{10}$, $\epsilon = 0.326$, the interior is quite warm, isothermal and almost isoviscous, however, when $\Delta\eta = 10^{16}$, $\epsilon = 0.2036$, the interior gets significantly cooler and the stagnant lid becomes thicker. Also there is a clear emergence of a high viscosity region in the lower mantle and this behaviour persists and becomes more prominent when $\Delta\eta = 10^{20}$ with $\epsilon = 0.163$. We assume that all these remarkable changes in the thermal distribution might explain the significant change in the values of Nu. We believe this indicates that the transition in the curves in Figure 8 is from a thermoviscous $\eta(T)$ regime of $\mu \sim \epsilon$ to a thermobaroviscous regime $\mu \gg \epsilon$.

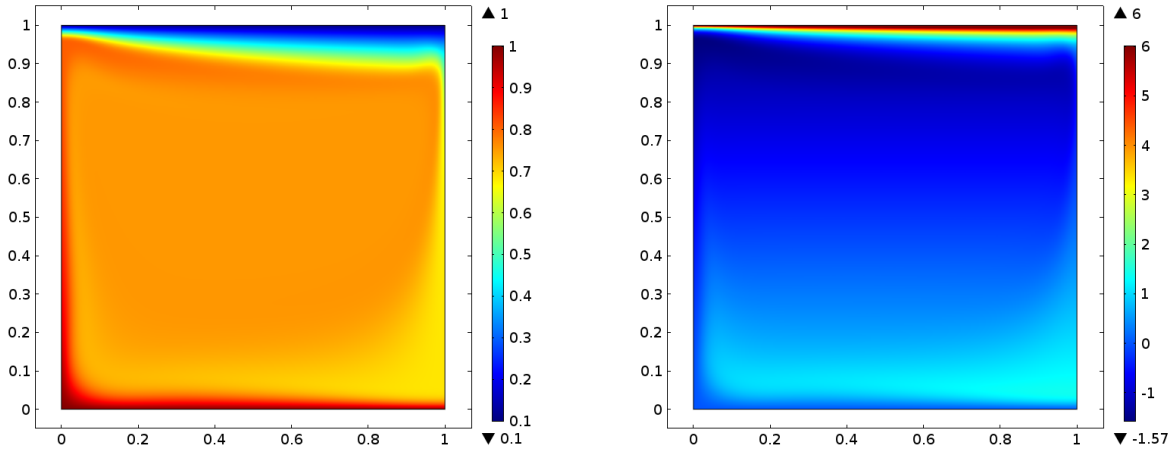

(*a*) $\Delta\eta = 10^{10},\ \mu = 1.5,\ \varepsilon = 0.326$

(*b*) $\Delta\eta = 10^{10},\ \mu = 1.5,\ \varepsilon = 0.326$

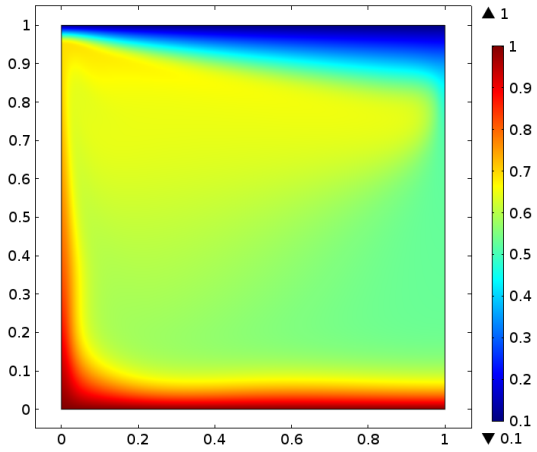

(*c*) $\Delta\eta = 10^{16},\ \mu = 1.5,\ \varepsilon = 0.2036$

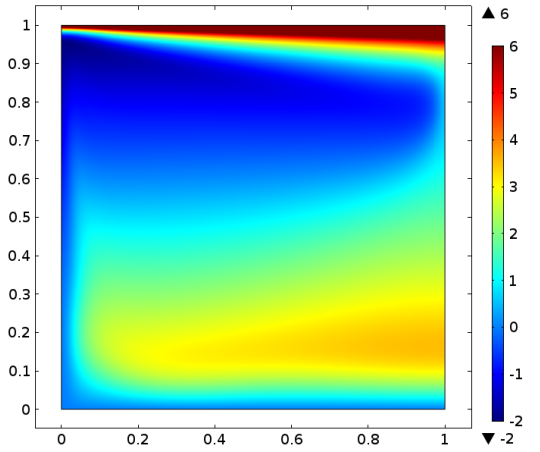

(*d*) $\Delta\eta = 10^{16},\ \mu = 1.5,\ \varepsilon = 0.2036$

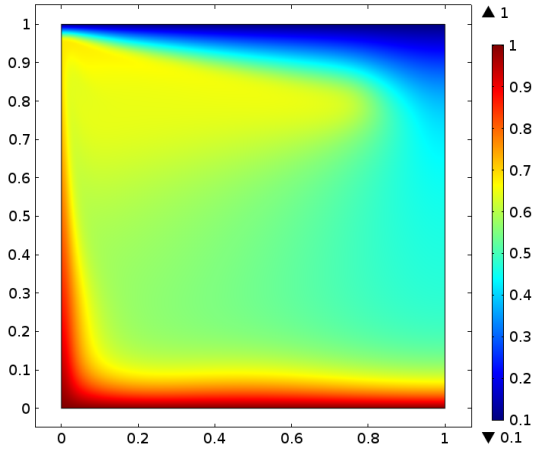

(*e*) $\Delta\eta = 10^{20},\ \mu = 1.5,\ \varepsilon = 0.163$

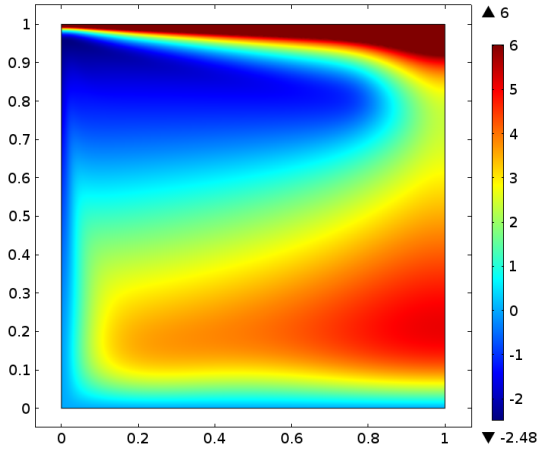

(*f*) $\Delta\eta = 10^{20},\ \mu = 1.5,\ \varepsilon = 0.163$

Figure 11: Temperature distributions (a, c, e) and the corresponding viscosity distributions (logarithm plots) (b, d, f) with different viscosity contrasts at a fixed pressure sensitivity $\mu = 1.5$, in a square cell with $T_0 = 0.1$ and $Ra = 10^7$.

5 Discussion and Comparison between 'with' and 'without' internal heating

To demonstrate the significant effects of including internal heating temperature profiles in the convecting cell at $\mu = 0.5$ and $\mu = 1.0$ with $H = 0.0$ are shown in Figure 12.

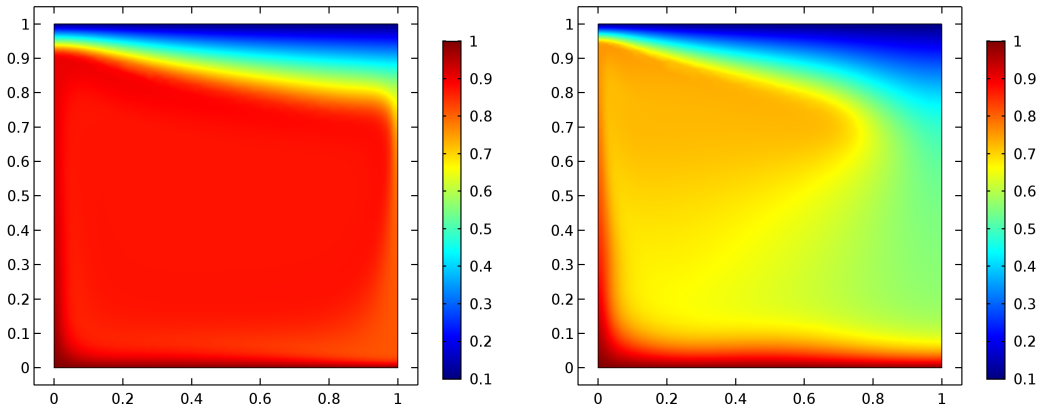

(a) $\Delta\eta = 10^{30}$, $\mu = 0.5$, $H = 0.0$ (b) $\Delta\eta = 10^{30}$, $\mu = 1.0$, $H = 0.0$

Figure 12: Thermal distributions of a temperature and pressure dependent viscosity convection without internal heating at $\mu = 0.5, 1.0$ with $\theta_0 = 0.1$ and $Ra = 10^7$.

In each plot the top thermal boundary layer forms an effectively rigid lid. However, in the rest of the cell the differences between Figure 12(a) and Figure 2(d) and between Figure 12(b) and Figure 4(d) are noticeable. When $\mu = 0.5$ the bulk fluid is roughly isothermal and isoviscous. We notice that at the lower mantle and near the core mantle boundary there is a very thin warm yellow region (right corner) whereas in Figure 2(d) we observe a red region indicating that the temperature is higher than Figure 12(a). When $\mu = 1$ it is no longer possible for the bulk flow to be both isothermal and isoviscous and we observe the emergence of a quite different characteristic flow structure, with relatively warm (yellow) upper mantle separated from a cooler (green) lower mantle (Figure 12(b)), whereas we notice a warm orange region in the upper mantle and relatively warm (yellow) region in the lower mantle (Figure 4(d)). Also the upper mantle region almost touches the right side of the cell.

From Table 3 and Table 4, we compare the values of Nusselt number and RMS velocity between $H = 0.0$ and $H = 6.0$ for $\mu = 0.5, 1.0$. By comparing between $H = 0.0$ and $H = 6.0$ we observe that, as the viscosity contrast increases the values of Nu and RMS

velocity decrease for both $\mu = 0.5, 1.0$ but when internal heating is added, both the Nusselt number and RMS velocity shows an irregular pattern of slowly decresing and increasing behaviour. However, root mean square velocity is significantly lower with internal heating for the case $\mu = 0.5$. But the effect is quite different for $\mu = 1.0$. Even though RMS velocity decreases with large viscosity contrast, the rate of decrease is slow, and hence we obtain higher values of RMS velocity with internal heating compared to no internal heating for the case $\mu = 1.0$.

6 Conclusions

The principal aim of this study has been to investigate the Rayleigh-Bénard convection with strongly temperature and pressure dependent viscous fluid relative to the mantle in the presence of internal heating at a very high Rayleigh number. We consider a two-dimensional model for convection in a unit aspect-ratio cell with free-slip boundary conditions with a low temperature cut-off viscosity function in addition of internal heating. The results we have found may have serious implications for the style of convection in the mantle of the Earth and other terrestrial planets. Purely basally heated convection in plane layers leads to upwellings and downwellings of equal intensity (equal and opposite thermal anomalies and velocities). However, one of the defining characteristics of convection in the Earth's mantle is that it is very likely powered by radiogenic heating from the decay of uranium, thorium and potassium distributed throughout the mantle (D. Turcotte & Schubert, 1982). Thus, the mantle is not only heated along the core-mantle boundary by the hotter molten iron outer core, it is also heated throughout its interior. This component of internal heating leads to a very significant breaking of the symmetry between upwellings and downwellings. We find that temperature and pressure dependence of the viscosity in the presence of internal heating results in a quite different flow regime, shown for example in Figures (2,4)(d), which is completely different from the flow profile when internal heating is neglected. However, the nature of the resulting convection can be understood if one realizes that the bottom thermal boundary layer must conduct in the heat injected through the bottom while the top thermal boundary layer must conduct out both the heat injected through the bottom as well as the heat generated internally (Bercovici et al., 2000). We observed that the temperature profile are quite different when internal heating is present. We have also investigated how pressure dependence parameter influences the heat transfer and found a relation with the order of temperature dependence parameter when the convection is purely basally heated.

It is obvious that inclusion of different factors will make the model more sophisticated and complex as well. We hope that our study has discovered some significant characteristics of convection with strong temperature and pressure dependent viscosity and with internal heating which are relevant to the mantle of the Earth and other terrestrial planets and give an insight of the broader picture of mantle convection in the Earth as well as other terrestrial planets.

Acknowledgments

Tania S. Khaleque acknowledges the valuable suggestions from Professor A. C. Fowler, University of Oxford, U.K.

References

Bercovici, D., Ricard, Y., & Richards, M. A. (2000). The relation between mantle dynamics and plate tectonics: A primer. *Geophysical monograph-american geophysical union.*, *121*, 5–46.

Bercovici, D., Schubert, G., & Glatzmaier, G. (1989). Influence of heating mode on three-dimensional mantle convection. *Geophysical Research Letters.*, *16*(7), 617–620.

Blankenbach, B., Busse, F., Christensen, U., Cserepes, L., Gunkel, D., Hansen, U., ... others (1989). A benchmark comparison for mantle convection codes. *Geophysical Journal International.*, *98*(1), 23–38.

Christensen, U. (1984). Heat transport by variable viscosity convection and implications for the earth's thermal evolution. *Physics of the Earth and planetary interiors.*, *35*(4), 264–282.

Christensen, U. (1984b). Convection with pressure-and temperature-dependent non-newtonian rheology. *Geophysical Journal International.*, *77*(2), 343–384.

Davies, G. F., & Richards, M. A. (1992). Mantle convection. *The Journal of Geology.*, *100*(2), 151–206.

Doin, M. P., Fleitout, L., & Christensen, U. (1997). Mantle convection and stability of depleted and undepleted continental lithosphere. *Journal of Geophysical Research: Solid Earth.*, *102*(B2), 2771–2787.

Dumoulin, C., Doin, M. P., & Fleitout, L. (1999). Heat transport in stagnant lid convection with temperature-and pressure-dependent newtonian or non-newtonian rheology. *Journal of Geophysical Research: Solid Earth.*, *104*(B6), 12759–12777.

Fleitout, L., & Yuen, D. A. (1984). Steady state, secondary convection beneath lithospheric plates with temperature-and pressure-dependent viscosity. *Journal of Geophysical Research: Solid Earth.*, *89*(B11), 9227–9244.

Fowler, A. C. (2011). *Mathematical geoscience* (Vol. 36). Springer Science & Business Media.

Houston, M., & De Bremaecker, J. C. (1975). Numerical models of convection in the upper mantle. *Journal of Geophysical Research.*, *80*(5), 742–751.

Huang, J., & Zhong, S. (2005). Sublithospheric small-scale convection and its implications for the residual topography at old ocean basins and the plate model. *Journal of Geophysical Research: Solid Earth.*, *110*(B5).

Huang, J., Zhong, S., & van Hunen, J. (2003). Controls on sublithospheric small-scale convection. *Journal of Geophysical Research: Solid Earth*, *108*(B8).

Ito, E., & Katsura, T. (1989). A temperature profile of the mantle transition zone. *Geophysical Research Letters.*, *16*(5), 425–428.

Jarvis, G. T., & Peltier, W. (1982). Mantle convection as a boundary layer phenomenon. *Geophysical Journal of the Royal Astronomical Society*, *68*(2), 389–427.

Jimenez, J., & Zufiria, J. A. (1987). A boundary-layer analysis of rayleigh-bénard convection at large rayleigh number. *Journal of Fluid Mechanics.*, *178*, 53–71.

Kameyama, M., & Ogawa, M. (2000). Transitions in thermal convection with strongly temperature-dependent viscosity in a wide box. *Earth and Planetary Science Letters.*, *180*(3-4), 355–367.

Khaleque, T. S., Fowler, A. C., Howell, P., & Vynnycky, M. (2015). Numerical studies of thermal convection with temperature-and pressure-dependent viscosity at extreme viscosity contrasts. *Physics of Fluids*, *27*(7), 076603.

King, S. D. (2009). On topography and geoid from 2-d stagnant lid convection calculations. *Geochemistry, Geophysics, Geosystems.*, *10*(3).

King, S. D. (2015). Mantle convection, the asthenosphere, and earth's thermal history. *Geological Society of America Special Papers.*, *514*, SPE514–07.

Koglin Jr, D. E., Ghias, S. R., King, S. D., Jarvis, G. T., & Lowman, J. P. (2005). Mantle convection with reversing mobile plates: A benchmark study. *Geochemistry, Geophysics, Geosystems.*, *6*(9).

Korenaga, J. (2017). Pitfalls in modeling mantle convection with internal heat production. *Journal of Geophysical Research: Solid Earth*, *122*(5), 4064–4085.

Leitch, A., Yuen, D., & Sewell, G. (1991). Mantle convection with internal heating and pressure-dependent thermal expansivity. *Earth and Planetary Science Letters.*, *102*(2), 213–232.

Limare, A., Fourel, L., Surducan, E., Neamtu, C., Surducan, V., Vilella, K., ... Jaupart, C. (2015). Microwave-based, internally-heated convection: New perspectives for the heterogeneous case. In *Aip conference proceedings* (Vol. 1700, p. 040001).

Moresi, L.-N., & Solomatov, V. (1995). Numerical investigation of 2d convection with extremely large viscosity variations. *Physics of Fluids.*, *7*(9), 2154–2162.

Olson, P., & Corcos, G. (1980). A boundary layer model for mantle convection with surface plates. *Geophysical Journal of the Royal Astronomical Society.*, *62*(1), 195–219.

Roberts, G. (1977). Fast viscous convection. *Geophysical & Astrophysical Fluid Dynamics.*, *8*(1), 197–233.

Schubert, G., Turcotte, D. L., & Olson, P. (2001). *Mantle convection in the Earth and planets.* Cambridge University Press.

Solomatov, V., & Moresi, L.-N. (1997). Three regimes of mantle convection with non-newtonian viscosity and stagnant lid convection on the terrestrial planets. *Geophysical Research Letters.*, *24*(15), 1907–1910.

Stein, C., Lowman, J., & Hansen, U. (2013). The influence of mantle internal heating on lithospheric mobility: Implications for super-earths. *Earth and Planetary Science Letters*, *361*, 448–459.

Stemmer, K., Harder, H., & Hansen, U. (2006). A new method to simulate convection with strongly temperature-and pressure-dependent viscosity in a spherical shell: Applications to the earth's mantle. *Physics of the Earth and Planetary Interiors.*, *157*(3-4), 223–249.

Turcotte, D., & Oxburgh, E. (1967). Finite amplitude convective cells and continental drift. *Journal of Fluid Mechanics.*, *28*(1), 29–42.

Turcotte, D., & Schubert, G. (1982). Application of continuum physics to geological problems. *NY: Wiley.*.

Turcotte, D. L., & Schubert, G. (2002). *Geodynamics.* Cambridge university press.

Van Heck, H., & Tackley, P. (2011). Plate tectonics on super-earths: equally or more likely than on earth. *Earth and Planetary Science Letters*, *310*(3-4), 252–261.